Materials Chemistry and Physics 243 (2020) 122571

Contents lists available at ScienceDirect

Materials Chemistry and Physics

journal homepage: www.elsevier.com/locate/matchemphys

Effects of oxidizing procedures on carbon nanofibers surface and dispersability in an epoxy resin

A. Romero [a], M.P. Lavin-Lopez [b], M.L. Sánchez-Silva [a], J.L. Valverde [a], A. Paton-Carrero [a,*]

[a] University of Castilla-La Mancha, Department of Chemical Engineering, Avenida Camilo Jose Cela 12, 13071, Ciudad Real, Spain
[b] Graphenano S.L., Calle Pablo Casals 13, 30510, Yecla, Murcia, Spain

HIGHLIGHTS

- Effective oxidation methods based on highly oxidative agents.
- Exfoliation and reduction process in order to reduce oxygen groups attached to the structure.
- Exhaustive characterization of all intermediate materials providing a useful repository of this different methods.
- Dispersibility study of oxidized carbon nanofiber into threedifferent solvernts.

ARTICLE INFO

Keywords:
Graphite
Graphene
Carbon nanofibers
Oxidation
Epoxy resin
Dispersion

ABSTRACT

Different oxygen functionalities were introduced in fishbone-type carbon nanofibers (CNFs) using three different oxidation procedures. The differences between these procedures are mainly based in the oxidizing agent used and the acid medium in which the process was carried out. Potassium permanganate-, ferrate- and chromate-based approaches were employed in conjunction with exfoliation and subsequent reduction with hydrazine. A complete evaluation of the effects produced by the different oxidative treatments on the resulting materials was carried out. The obtained materials were characterized by Scanning Electron Microscopy (SEM), EDX, RAMAN, Fourier Transform Infrared (FTIR), X-ray diffraction (XRD), N_2 adsorption/desorption measurements, particle size and thermogravimetric analysis. The results suggest that only those procedures in which H_2SO_4 was used as acid medium (i.e., potassium permanganate and ferrate processes) were fit to achieve intercalation of suitable species (SO_4^{2-} ions) that weaken the van der Waals forces. The weakening of these forces facilitates the attack of the carbon skeleton by the strong oxidants MnO_4^- or $FeO_4^{2-}$and, as a consequence, the fragmentation of the material occurs. Dispersibility of carbon materials are affected by functional groups and oxidation degree. Turbiscan stability index provide a useful tool in order to study the stability of carbon material into different solvents with different dipole moments: water, epoxy resin and decane.

1. Introduction

Carbon nanofibers (CNFs) are characterized by their high degree of orientation of their graphitic basal planes respect to the fiber axis and their unique mechanical, electronic and thermal properties. These materials have attracted significant attention in recent years due to the wide range of potential applications in which they can be used, such as sensor manufacture, energy storage, nanocomposites etc. [1]. CNFs are defined as cylindrical graphitic nanostructures in which the graphite layer can be arranged in various ways. These compounds can be classified as *ribbon*-type CNFs with layers of graphene parallel to the fiber axis, *fishbone*-type CNFs with layers of graphene aligned at an angle to the fiber axis, *cup stacked-up*-type CNFs with truncated cones stacked up in the direction of the fiber axis, and *spiral helix*-type CNFs with a continuous layer of graphene aligned with the axis in helical manner [2].

Epoxy is one of the most important polymers used in a wide range of applications (adhesive, electronic devices, surface coating, sport gears, automobile, anti-corrosive.) due to the large amount of inherits properties and the non-expensive production [3]. However, epoxy structure presents other properties which limit the use of this material on mechanical applications [4]. In this sense, several nanomaterials have been

* Corresponding author.
E-mail address: Antonio.Paton@uclm.es (A. Paton-Carrero).

https://doi.org/10.1016/j.matchemphys.2019.122571
Received 25 July 2019; Received in revised form 27 November 2019; Accepted 22 December 2019
Available online 23 December 2019
0254-0584/

studied due to the properties provided to this resin which can empower it for mechanical or even multi-functional applications [5]. In general, dispersion of nanofiller is a key problem in nanotechnology and, therefore, it can be considered an integral aspect in polymer nanotechnology field [6]. In general, nanofillers have a high surface to volume ratio which in addition to the number of particle-matrix interactions increasing in effects of the nanofiller properties on the whole. Composite materials that combine high strength nanofibers reinforced plastics, are used in automobile and aerospace industries as high strength and lightweight materials. Nevertheless, the use of oxidized carbon nanofibers with this purpose has not been depth studied. Thus, functionalization of carbon nanofibers by oxidation treatments could be used to improve the interactions strength between the carbon fiber and the resin obtaining well dispersed nanostructures, providing new enviable nanocomposite characteristics [7–9].

Several methods have been proposed for the oxidation of carbon nanofibers (or other graphene-based materials) and it is worth highlighting CNFs intercalation either with metal ions or by acid oxidation treatments [10,11]. When an acid oxidative treatment is employed, a further exfoliation treatment yields the (oxidized) carbon nanomaterial. A subsequent reduction step leads to the reduced carbon nanomaterial. In the present work, CNFs were oxidized by treatments with different strong acids and oxidants. The most important step in this method is based on weakening the van der Waals forces between the graphene sheets of the carbon nanofibers by intercalating certain species between them with the aim of introduce functional groups easily.

Although it is clear that the use of different oxidation routes has an impact on the properties of the final product (nature of the oxygen functionalities, sheet size, number of defects, sp^2 and sp^3 domains, etc. [12]), there are very few studies in which all or several such properties have been evaluated. In this context, the study reported here highlights new acid oxidation procedures for carbon nanomaterials that employ novel conditions and/or oxidants subsequent exfoliation and, finally, chemical reduction with hydrazine. In this sense, three different routes were followed: the well-known *Improved Hummers Method* [13,14], a new and environmentally friendly fast and economic method based on the use of *Potassium Ferrate* as the oxidizing agent along with H_2SO_4 which avoids the use of $KMnO_4$ as an oxidizing agent due to its high toxicity, and, finally, a novel method based on the use of a mixture of perchloric and nitric acids and potassium chromate as the oxidizing agent [15].

The employed acid oxidation procedures employed are quite similar to those used to produce graphene oxide because it has been demonstrated in different studies that acid oxidative treatments are more efficient if they are applied to materials in which the number of carbon layers is lower, such as CNFs [11]. The effects that both the oxidation power inherent in the oxidizing reagent (potassium permanganate, ferrate and chromate) and the acid media had on the morphology, pore structure, crystallinity, surface chemical properties and thermal properties of the resulting products were analyzed in detail. In addition, an exhaustive dispersibility analysis of the resulting oxidized materials on epoxy resin (compared to other solvent such as polar water and apolar decane) was performed in order to analyze the consequence of the oxidation on the nanomaterial stability.

2. Experimental

2.1. Materials

$KMnO_4$ (purity of 99%), H_2SO_4 (purity of 96%), hydrazine monohydrate (NH_2–NH_2) and HCl (purity $\geq$ 37%) were supplied by Sigma-Aldrich. H_2O_2 (purity of 33%), ethanol (purity of 99.5%) and K_2CrO_4 were supplied by Panreac. K_2FeO_4 (purity of 92%) was supplied by Lab Seeker, n-decane was distributed by Fluka and commercial epoxy resin was RESOLTECH 1020 supplied by Castro Composites.

2.2. Oxidation of carbon nanofibers (O-CNFs)

Raw CNFs were synthesized by the CVD method following the procedure developed by Jimenez et al. [16].

CNFs were first oxidized using potassium permanganate ($KMnO_4$) as the oxidizing agent according to the well-known *Improved Hummers' method* with some modifications [14]. The experimental procedure is detailed below. 15 g of carbon nanofibers were mixed with 45 g of potassium permanganate ($KMnO_4$). This mixture was carefully added to 400 ml of sulfuric acid (H_2SO_4) under vigorous agitation. After the addition was complete, the solution was stirred at 50 °C for 3 h in order to complete the graphite oxidation. The mixture was allowed to cool and was drowned out into 400 g of flake ice and 3 ml of H_2O_2. Hydrogen peroxide stops the oxidation process and flake ice prevents an increase in the solution temperature caused by the exothermic reaction. The solid was filtered off under vacuum and washed with 200 ml of deionized water, 200 ml of hydrochloric acid (to dissipate the metallic ions) and, 200 ml of ethanol (to improve the drying process). The compact cake was dried at 100 °C for several hours. The CNF sample produced by this method was denoted as O-CNFs Permanganate.

The Ferrate-method for CNF oxidation was carried out by mixing 10 g of CNFs and 60 g of potassium ferrate (K_2FeO_4) and adding this mixture to 400 ml of concentrated sulfuric acid. The solution was stirred continuously for 1 h at room temperature. After 1 h the solid was filtered off under vacuum. The cake was washed with distilled water until neutral pH and dried for 3 h at 80 °C [17]. Carbon nanofibers oxidized by this method were denoted as O-CNFs Ferrate.

Finally, carbon nanofibers were oxidized using potassium chromate (K_2CrO_4) as the oxidizing agent. In this method, the acid solution was composed of 150 ml of nitric acid and 200 ml of perchloric acid. A mixture of 6 g of graphite and 18 g of potassium chromate (1:3) was added to the acid solution. The reaction took place at 100 °C under vigorous stirring for 24 h. The solid was filtered off under vacuum and washed with deionized water, hydrochloric acid and ethanol (200 ml each). The cake was dried at 80 °C for 4 h [15]. Carbon nanofibers oxidized by this method were denoted as O-CNFs Chromate.

2.3. Exfoliation of carbon nanofibers (Ex-CNFs)

The exfoliation process was carried out by sonication of the oxidized carbon nanofibers. The sonicated solution consisted of 800 mg of O-CNFs in 800 ml of distilled water. This solution was transferred to a reactor with a cooling jacket in order to avoid a significant temperature increase. Sonication was carried out for 2 h, after which time the graphene layers present in O-CNFs began to separate. The solid from the sonicated solution was then filtered off and dried at 80 °C for 2 h to give the product denoted as Ex-CNFs.

2.4. Reduction of carbon nanofibers (r-CNFs)

Hydrazine monohydrate was selected to carry out the chemical reduction. For the reduction, 800 mg of hydrazine was diluted with 800 ml of 1 g/L Ex-CNFs solution. The solution was stirred at 90 °C for 3 h. After this time, the solid was filtered off under vacuum and washed several times to remove the remaining hydrazine. Finally, the powder was dried at 80 °C for 2 h.

2.5. Dispersion stability analysis

Turbiscan™ Lab Expert was used for analyzing the stability of suspensions. The principle of measurement is based on transmission and backscatter detectors. The stability of suspensions of raw CNF and all O–CNF in water, n-decane and the commercial epoxy resin "RESOLTECH 1020" was studied. For this purpose, 100 mg of both raw CNF and O–CNF were dispersed into 100 ml of the three different solvents above listed. The suspension was mechanically stirred for 60 min at 300 rpm

until the complete solute dispersion in liquid matrix was achieved. Then, the mixture was sonicated for 60 min more. Finally, the dispersion was transferred to 20 ml cylindrical vials which were subsequently placed into the instrument. Stability runs were performed at 30 °C for 48 h. Data and more specifically the Stability Index (TSI) provided by the instrument and were recorded each 30 min. TSI parameter consider that any destabilization phenomenon happening in a given sample will have an effect on the BackScattering and/or Transmission signal intensities during time. The equation that follows TSI values are:

$$TSI = \frac{\sum_h |scan_i(h) - scan_{i-1}(h)|}{H} \quad (1)$$

This index is a direct measure of the destabilization kinetics of a suspension. The smaller the variation in value of the TSI, the higher the stability of the suspension.

2.6. Characterization techniques

The morphology of the different samples was evaluated by Scanning Electron Microscopy (SEM) (*Phenom ProX*) and elemental analysis was carried out using the EDX software of the SEM equipment. Fourier transform infrared (FTIR) spectra were obtained on a *SPECTRUM TWO* spectrophotometer (PerkinElmer) in transmission mode using KBr (350-8300 cm^{-1}) pellets and ZnSe (550–6000 cm^{-1}). Thermogravimetric analysis (TGA) data were recorded on a *METTLER TOLEDO TGA/DSC1* instrument using a heating rate of 10 °C min^{-1} in air. Raman spectra were obtained by a SENTERRA spectrophotometer using an excitation wavelength of 532 nm. The particle size was measured using a Mastersizer 2000 module -Hydro-. Surface area/porosity measurements were made using a Quantachrome Quadrasorb SI apparatus with N_2 as the sorbate at 77 K. All samples were outgassed prior to analysis at 453 K under vacuum (1×10^{-2} Torr) for 18 h. Total specific surface areas were determined by the multipoint BET method. The powder X-ray diffraction (XRD) analyses were performed on a diffractometer (PHILIPS, PW-1711) with CuKα radiation (λ = 1.5404 Å). Characteristic crystallographic parameters (interlaminar space (d002) and the in-plane crystallite size or layer size (L_a)) were determined as follows [18,19]:

$$d_{002} = \frac{\lambda}{2 \cdot sen\theta_1};$$

$$La(nm) = \frac{k_1 \cdot \lambda}{FWHM \cdot \cos\theta_2}$$

where:

- λ, radiation wavelength (λ = 0.15404 nm)
- θ_1, [002] and [001] diffraction peak position (°)
- θ_2, [100] diffraction peak position (°)
- k_1, Warren Form Factor constant (k = 1.84)
- *FWHM*, Width at half maximum height of the corresponding diffraction peak (rad)

3. Results and discussion

3.1. Materials characterization

Oxidized (O-CNFs), exfoliated (Ex-CNFs), and reduced carbon nanofibers (r-CNFs) were prepared and studied in detail in the present after three different oxidative processes in which three oxidizing agents were employed (potassium permanganate, potassium ferrate and potassium chromate).

The elemental analysis data, i.e., the oxygen and carbon contents (wt.%), for the different materials are provided in Table 1. The non-oxidized raw CNFs are composed of 86% carbon and 11% oxygen. In general, CNFs, mainly those synthesized by the CVD method, have a significant lack of conjugation and numerous dangling bonds are present. These materials therefore, have a significant density of defects and these allow etching to occur, even under relatively mild oxidation conditions [20]. The silicon residues observed in the elemental analysis were due to the support (SiO_2) used in the CNF synthesis (traces of Ni were also observed in the analyses but are not included in Table 1 as their values were very low). After the oxidation process, different oxygen contents of around 33%, 22% and 18% were measured in samples oxidized using the permanganate, ferrate and chromate procedure, respectively. After exfoliation by sonication, a similar oxygen content to that obtained for O–CNF samples was obtained regardless of the oxidative process [21]. Finally, after the chemical reduction process with hydrazine, the oxygen content was reduced to 24%, 13% and 11% in samples treated using permanganate, chromate, and ferrate procedure, respectively.

Table 1
Atomic composition corresponding to oxidized, exfoliated and reduced CNFs.

Raw material		*Product*	*C (%)*	*O (%)*	*Si (%)*
		CNFs	85.2	10.9	3.9
OXIDATIVE TREATMENT	Ferrate	O-CNFs	76.9	21.5	3.6
		Ex-CNFs	76.2	20.2	3.6
		r-CNFs	88.5	11.0	0.5
	Chromate	O-CNFs	78.3	17.8	3.9
		Ex-CNFs	80.4	16.7	2.9
		r-CNFs	83.9	13.5	2.6
	Permanganate	O-CNFs	63.9	32.6	3.6
		Ex-CNFs	64.1	32.0	3.8
		r-CNFs	74.8	24.2	1.0

As observed from the results, the procedure based on CNF oxidation using permanganate was the most efficient in terms of incorporation of oxygen functional groups in the CNF structure, being followed by the ferrate procedure. The influence that the incorporation of different functional oxygen groups in the CNF structure has on properties such as crystallinity, thermal resistance, pore structure, particle size, etc. is discussed in detail below.

In order to discern the oxidation process which take place during the reaction, the mechanism pathway for three oxidation has been explained. During the permanganate reaction (reaction 1 and 2) the oxidation of carbon nanofibers takes places with the reduction of permanganate ions into permanganate bimetallic heptoxide in a sulfuric acid matrix [22]. This bimetallic heptoxide is more reactive than the other monometallic counterparts. This molecule provide an extremely explosive reaction in organic carbon presence oxidizing the unsaturated carbon double bonds.

$$KMnO_4 + H_2SO_4 \rightarrow K^+MnO_3^+ + 3HSO_4^- \quad (2)$$

$$MnO_3^+ + MnO_4^+ \rightarrow Mn_2O_7 \quad (3)$$

The oxidizing method which involves ferrate (reaction 2) are able to oxidize the carbon atoms in two identical steps using the oxygen molecules generated during the water production and the iron (VI) reduction [17].

$$C(CNF) + FeO_4^{2-} \rightarrow ox - C(CNF) + Fe^{3+} + H_2O \quad (4)$$

The last mechanism with chromate is a well-known reaction used in alcohol oxidation (reaction 4). The potassium chromate turns into potassium dichromate in aqueous solution. The dichromate in acid presence reduces to Cr (III), this reduction has an enormous oxidation potential (+1.6 eV) which allow the carbon atoms of nanofibers to oxidize.

$$Cr_2O_7^{2-} + 14H^+ + 6e^- \rightarrow 2Cr^{3+} + 7H_2O \quad (5)$$

In order to obtain information about the nature of oxygenated functional groups, infrared analysis (FTIR) of powdered samples was carried out and their spectra are shown in Fig. 1. It can be seen that, after oxidation with the different agents, several functional groups were introduced into the structure of the raw CNFs. A broad band in the range 3000–3600 cm^{-1}, corresponding to ordered OH stretching vibrations of hydroxyl groups coordinated to the CNF surface [21], can be appreciated in CNFs treated using the chromate-based method. The peak centered at around 3600 cm^{-1} present in the spectra of samples treated with ferrate or permanganate is assigned to disordered OH stretch, due to weakly bound surface hydroxyls with possible lateral interactions between them (e.g. H bonding) [23,24]. Bands located at around 3010 cm^{-1} corresponding to alkene groups (C–H) and bands in the range 2850–2950 cm^{-1} (and also at low wavelength values of 850 cm^{-1}), corresponding to CH_2/CH_3 stretching vibrations, are indicative of oxidized CNFs having a defect-rich structure with carbon-hydrogen bonds [25]. These latter bands were more prominent in samples oxidized using the ferrate- and permanganate-based oxidative treatments and, as a consequence, bands at around 1650 cm^{-1}, attributed to the C=C skeletal vibration of the graphene planes (unoxidized domains) [26], were only clearly appreciated in samples oxidized using the chromate-based method. Carboxyl O–H groups, which give rise to bands at around 1420 cm^{-1} [27], were observed in all samples regardless of the oxidizing agent used. This finding is important from the practical standpoint, because these groups easily couple to a variety of reagents and polymers for multiple applications [28]. A peak at around 1220 cm^{-1}, attributed to the stretching vibration of an epoxy CO–O–CO group, was clearly visible in samples oxidized by the permanganate and ferrate methods, thought considerably weaker in sample oxidized by treatment with chromate. Finally, an intense band around 1050–1150 cm^{-1} is present for all samples and this is attributed to C–O stretching vibrations (ether bridges between rings, phenol, ester or aromatic acid, alcohol) [26,27].

As expected, FTIR identified similar functional groups in oxidized and exfoliated samples, thus confirming that the chemical identity of the bulk materials was not altered after sonication. Nevertheless, after reduction the main bands related to oxygen functional groups were partially reduced, although strong ordered O–H groups incorporated in the CNF structure after oxidation using the chromate-based method were only partially removed. In addition, the FTIR bands associated with C–H alkene and CH_2/CH_3 groups were present after reduction regardless of the oxidative treatment used.

It is important to note that the nature of the oxygenated groups incorporated in the CNF structure after oxidation using both

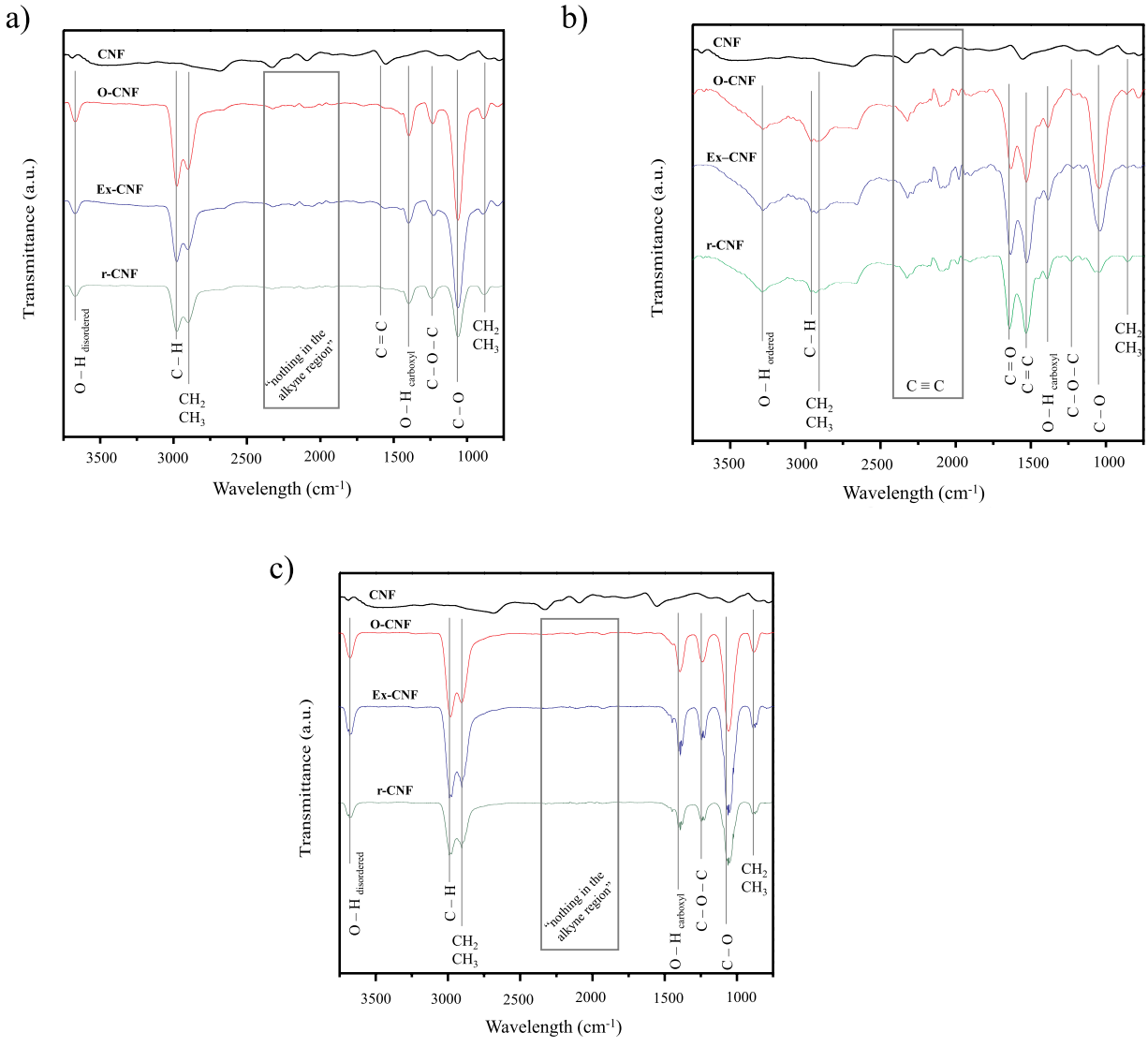

Fig. 1. FTIR spectra of raw CNFs and the corresponding CNF samples after oxidation using different procedures, exfoliation and reduction: a) ferrate, b) chromate, and c) permanganate procedure.

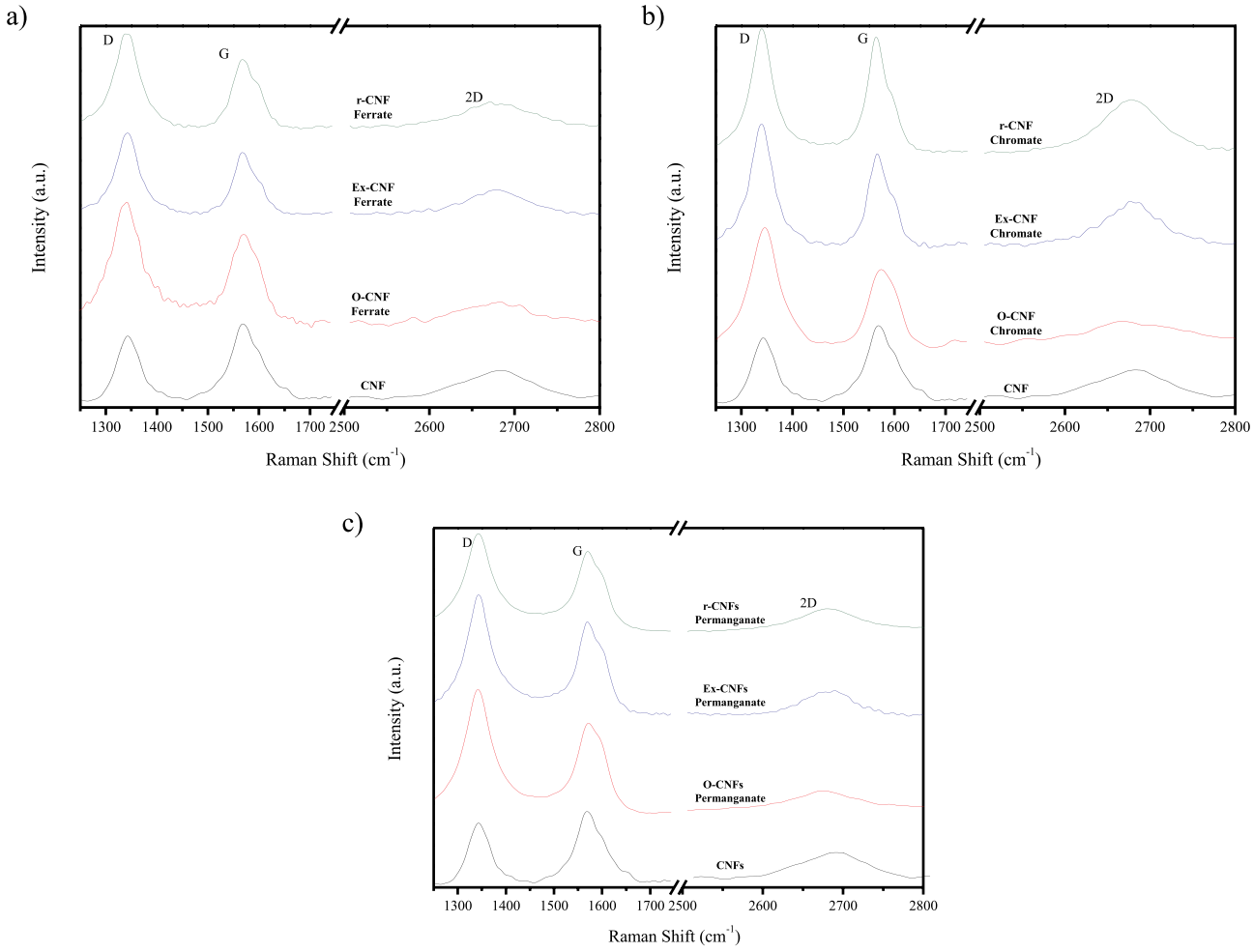

Fig. 2. First and second order Raman spectra for raw CNFs and the corresponding CNF samples after oxidation using different procedures, exfoliation and reduction: a) ferrate, b) chromate, and c) permanganate procedure.

permanganate- and ferrate-based methods was very similar, although the oxidation degree was considerably higher in sample oxidized using permanganate. However, the typology of these oxygen groups differs considerably from those observed in the structure of CNFs after oxidation using the chromate-based method. In other words, all evidence seems to indicate that the attack on the carbonaceous structure, which takes place during the oxidation process, was similar for the oxidative treatments based on the use of permanganate and ferrate as oxidizing agents, but it differed markedly from the structural attack by the chromate.

RAMAN spectroscopy provides important information about crystallographic and vibrational aspects of carbon materials. The Raman spectra of raw CNFs and those obtained after oxidation, exfoliation and reduction processes are shown inFig. 2. First order spectra (2D order in graphitic structures) include two peaks: the G band at around 1570 cm^{-1}, which originates from in-plane tangential stretching of sp^2 carbon-carbon bonds in graphene sheets (graphitic order), and the D band at around 1340 cm^{-1} arising from a double resonance Raman scattering process from a non-zero center phonon mode (in other words, structural imperfections in the carbon basal plane or edge site or those caused due to finite sized crystallites) [29,30]. A shoulder in the G band centered at around 1600 cm^{-1} (D′ band) implies disorder and defects as a consequence of intercalated compounds between graphene layers and/or oxidized sp^2 carbons [31,32]. The D′ band decreased as the degree of order increased [33]. In the second order Raman spectra it is worth highlighting the 2D band, which is a broad peak centered at around 2670–2680 cm^{-1} that, in the case of CNFs, overlaps with the band associated with amorphous carbon (centered at 2650 cm^{-1}) [34].

The ratio of the peak intensity of the D-band to that of the G-band (I_D/I_G) shown in Table 2 indicates the average size of the sp^2 graphitic domains and it is therefore related to the amount of defect sites present in the samples [35]. The raw CNF sample, with a high edge to basal planes ratio when compared to other carbon materials such as graphite, has a quite low crystallinity or high density of defects. As observed, after oxidation and exfoliation, an increase in the I_D/I_G ratio was observed and this indicates that the number of defect sites on the structure of O–CNF samples increased as a consequence of the introduction of the different oxygen groups, which in turn modified the hybridization of the surface carbon atoms towards greater sp^3 character. All of the oxidative treatments led to an increase in the I_D/I_G ratio to a similar extent, a fact that might seem strange since given that the sample oxidized by the chromate-based method (with an oxidation degree lower than the rest) would be expected to have fewer defects in its structure. The results seem to indicate that the oxygen functional groups present in the sample oxidized with chromate (with the lowest oxygen content), which is different in nature to those present in samples oxidized with the other oxidants (as corroborated by FTIR), were also responsible of the appearance of defects and imperfections in the original carbonaceous structure. In this sense, the explanations for the D and G band variations associated with oxidized samples could be different. In the case of the sample treated with chromate, the increase in the I_D/I_G ratio could be evidence of disruption of the aromatic system due to the attachment of

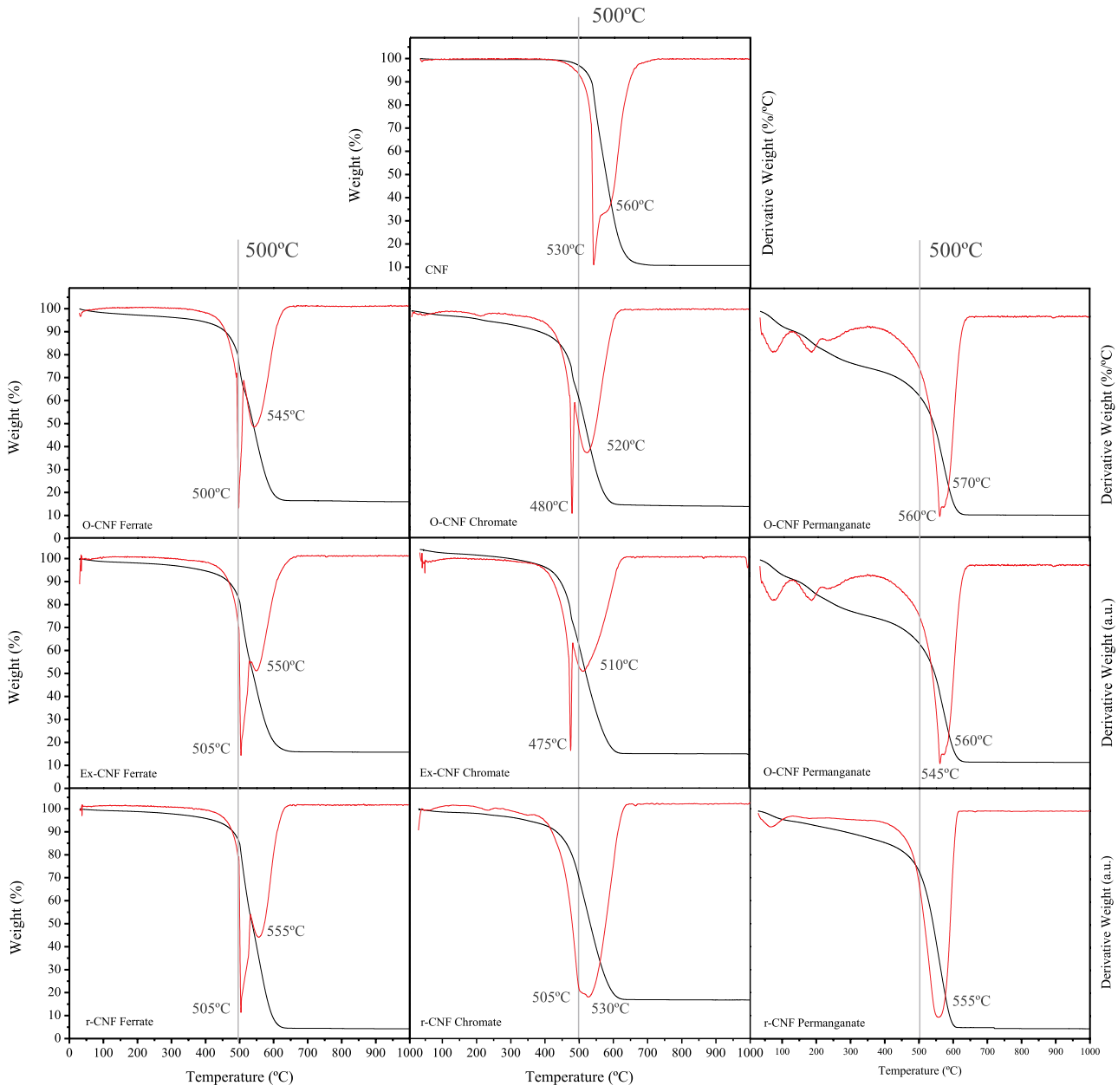

Fig. 3. TGA profiles of raw CNFs and the corresponding CNFs samples after oxidation using different procedures, exfoliation and reduction.

Table 2
Raman parameters: peak positions, FWHM, I_D/I_G and, I_{2D}/I_G of raw CNFs and the corresponding CNF samples after oxidation using different procedures, exfoliation and reduction: a) ferrate, b) chromate, and c) permanganate procedure.

		Product	D BAND	G BAND		2D BAND		VARIABLE
			FWHM(°)	POSITION (cm^{-1})	FWHM (°)	POSITION (cm^{-1})	FWHM (°)	I_D/I_G
Raw material		*CNFs*	*55*	*1574*	*66*	*2681*	*106*	*0.8*
OXIDATIVE TREATMENT	Ferrate	O-CNFs	75	1579	75	2673	88	1.3
		Ex-CNFs	53	1570	60	2676	78	1.3
		r-CNFs	60	1570	61	2674	117	1.4
	Chromate	O-CNFs	68	1580	70	2666	105	1.5
		Ex-CNFs	51	1570	59	2677	77	1.4
		r-CNFs	55	1569	52	2675	81	1.1
	Permanganate	O-CNFs	70	1580	70	2671	91	1.4
		Ex-CNFs	54	1572	60	2678	79	1.3
		r-CNFs	60	1573	63	2679	73	1.2

oxygen molecules. Nevertheless, in the case of permanganate and ferrate treatments, the destruction of the graphitic integrity and subsequent fragmentation of the graphitic structure could be the most plausible explanation [33]. These assertions are consistent with the FTIR results. On the other hand, after reduction with hydrazine, the I_D/I_G ratio was maintained or slightly decreased, which indicates that structural defects persisted despite the fact that some oxygen functional groups were removed.

The G band position and FWHM also serve to measure indirectly the in-plane structural order of the material [36]. In general, the higher the position (cm^{-1}) and width of the G-band, the lower the structural order and crystallinity [37]. The clear increase in both parameters after oxidation (regardless of the oxidizing agent) compared to that of raw CNFs again revealed the greater sp^3 character of the oxidized samples. It can also be appreciated that the D′ intensity increased after oxidation, mainly with the use of permanganate- and ferrate-based methods. These trends, together with the flattening of the 2D band, could indicate that the three-dimensional order of the graphene sheets in raw CNFs decreased due to the bi-dimensional disorder generated. In other words, the results confirm that amorphization or crystallinity loss took place during oxidation. Nevertheless, after exfoliation – and mainly after hydrazine reduction – the D′ band seemed to be smaller compared to that of O–CNF samples. The I_{2D}/I_G ratio clearly decreased after oxidation but it was recovered after exfoliation and, mainly, after reduction as a consequence of the rearrangement of the carbon lattice.

In order to corroborate both the RAMAN and FTIR results, thermogravimetric analyses were carried out (Fig. 3 and Table 3). The first weight loss, observed in the temperature range below 150 °C, was attributed to the evaporation of water molecules from the CNF surface. The TGA curve of CNFs confirmed the moderate thermal stability of this nanostructure, which did not start to decompose until around 500 °C and had lost around 88% of its mass at 670 °C. The rapid weight loss starting above 500 °C was mainly due to degradation or the thermal oxidation of the disordered carbon structure [38], although the oxygen functionalities strongly attached to the CNF structure were also degraded above 500 °C.

After the oxidation process, a significant weight loss took place in the temperature range between 150 and 500 °C (not observed in the raw CNFs) due to decarboxylation and removal of different oxygen functionalities. CNFs oxidized using the permanganate and chromate procedures showed a greater weight loss in the range 150–500 °C than the CNFs oxidized using ferrate. In this regard, and considering the FTIR results, the weight loss between 150 and 500 °C in oxidized CNFs using ferrate and permanganate could be associated mainly with the partial decarboxylation of C–O and disordered –OH groups (differences observed in the weight loss between both samples are due to the greater oxidation degree of the permanganate oxidized sample). Nevertheless, for the sample oxidized with chromate, it would also include the partial elimination of the ordered hydroxyl (–OH) groups. As observed from the results in Table 3, after exfoliation by sonication, thermal degradation of the carbon nanomaterial in the temperature range 150–500 °C decreased, thus increasing thermal degradation at temperatures above 500 °C (this fact was more pronounced in the sample obtained using the permanganate-based oxidative treatment, which had the highest oxidation degree). Taking into account that the oxygen content did not change after the sonication process (Table 1), it can be concluded that the morphological changes that took place after exfoliation (by sonication) were responsible for the strongest anchorage of the oxygen groups to the carbon structure in the exfoliated samples and, for this reason, their removal occurred at higher temperatures.

Finally, after the reduction process, thermal changes were mainly observed at temperatures above 500 °C, with a higher weight loss observed upon thermal degradation (the weight loss in the 150–500 °C temperature range remained unchanged with respect to Ex-CNF samples). In the case of the carbon nanofibers oxidized using chromate, a decrease in the weight loss between 150 and 500 °C was also observed, which indicates that the attack of hydrazine mainly reduced the oxygen groups that were weakly anchored to the carbon structure. These groups were degraded at temperatures below 500 °C, in contrast to samples oxidized using permanganate and ferrate. This fact can be clearly corroborated by the DTG profiles shown in Fig. 3, which usually show the temperature of the maximum rate of weight loss. It was observed that, most of the oxygen groups incorporated in the CNFs structure oxidized using the chromate-based method were degraded at temperatures below 500 °C, while oxygen functional groups incorporated in samples treated with permanganate and ferrate were degraded at temperatures above 500 °C. In this sense, and taking into account the FTIR results, the oxygen groups that were more strongly anchored to the CNFs structure, i.e., those that were therefore more thermally stable, would be mainly carboxyl and epoxy groups [21].

The residue observed in all samples was mainly due to the catalyst support and metal oxides derived from the CNFs synthesis. After permanganate and/or ferrate oxidation and exfoliation, the CNFs structure undergoes changes that allow the hydrazine used in the reduction process to attack the residue and remove it, an occurrence not observed when the oxidation process was carried out with chromate. This fact was corroborated by the FTIR results explained above, which demonstrate that –C═C– and –C≡C– bonds (present in the raw CNFs) were not observed after the oxidative treatment.

Nitrogen physisorption measurements were carried out in order to obtain information about the CNFs textural properties after oxidation, exfoliation and reduction (Table 4). A quantitative evaluation of the particle size of each sample dispersed in water (using a particle size analyzer) and the most significant XRD characteristic parameters are shown in Table 4. The results suggest that the oxidation treatment modified the mesoporous structure of the raw CNFs with the consequent decrease of both surface area and pore volume [39]. As can be observed, the external surface area clearly decreases after oxidation, probably due to the destruction of the smaller mesopores present in the original CNFs, which caused a significant increase in the average pore size. It is worth noting that the variation of the textural characteristics depending on the oxidizing agent is consistent with the oxidation degree obtained with each of them (Table 1). The mean crystallite layer size (LA) decreased significantly after the oxidation process only when permanganate- and

Table 3
TGA weight loss (% wt.) over different temperature ranges for raw CNFs and the corresponding CNFs samples after oxidation, exfoliation and reduction.

Raw Material		Product	0–150 °C	150–500 °C	>500 °C	RESIDUE
		CNFs	1	3	84	12
OXIDATIVE TREATMENT	Ferrate	O-CNFs	2	21	62	15
		Ex-CNFs	2	16	66	16
		r-CNFs	1	16	80	3
	Chromate	O-CNFs	3	47	35	15
		Ex-CNFs	2	40	43	15
		r-CNFs	2	30	50	18
	Permanganate	O-CNFs	3	46	36	15
		Ex-CNFs	4	24	55	17
		r-CNFs	4	24	68	4

Table 4
Particle size distribution, XRD parameters and textural properties of raw CNFs and samples after oxidation using different procedures, exfoliation and reduction.

	PRODUCT		PARTICLE SIZE		XRD		N_2 ADSORPTION/DESORPTION				
			$D_{0,5}$ (μm)	$D_{0,9}$ (μm)	d_{002} (nm)	L_A (nm)	SURFACE AREA (m^2/g)	EXTERNAL SURFACE AREA (m^2/g)	INTERNAL SURFACE AREA (m^2/g)	TOTAL PORE VOLUME (cc/g)	AVERAGE PORE SIZE AT P/P0 = 0.99 (nm)
	CNFs		49	125	0.343	15.0	132	127	5	0.39	5.9
OXIDATIVE TREATMENT	Ferrate	O-CNFs	60	143	0.344	6.2	100	92	8	0.35	7.2
		Ex-CNFs	41	85	0.345	4.4	130	103	27	0.35	5.6
		r-CNFs	63	125	0.348	4.1	113	90	23	0.37	7.1
	Chromate	O-CNFs	61	130	0.344	15.8	119	108	11	0.39	6.5
		Ex-CNFs	60	150	0.344	14.5	128	115	13	0.39	5.6
		r-CNFs	47	90	0.344	13.9	121	111	10	0.39	6.5
	Permanganate	O-CNFs	88	174	0.343	6.3	76	73	3	0.28	7.3
		Ex-CNFs	79	136	0.344	5.0	127	89	38	0.28	4.4
		r-CNFs	108	204	0.345	4.5	118	87	31	0.27	4.7

d_{002}: interlayer distance obtained by XRD. L_A: medium crystallite layer size obtained by XRD. D_{50} and D_{90} are particle sizes at which the percentages 50% and, 90% of the sample are below this given size.

ferrate-based methods were used. In contrast, this crystallographic variable was not affected when chromate was used as the oxidizing agent. This finding could again be due to the fact that this last oxidation process did not significantly affect the carbonaceous skeleton of the original CNFs. According to the results, it could be said that the inclusion of oxygen functional groups by treatments based on the use of permanganate and ferrate caused CNFs amorphization, with the development of smaller structures composed of defective graphene sheets with a low crystallite layer size.

Once the porous structure of the raw carbon nanomaterial has been weakened, the sonication process (exfoliation) opens it up, thus increasing the surface area and generating both external and internal porosity. Moreover, the structure continues to fragment (LA values decrease even more) and the average pore diameter was considerably reduced. After the reduction process, the surface area decreased slightly and, consequently, an increase in average pore size was observed.

The observed decrease in the total pore volume of the oxidized samples treated with ferrate and especially with permanganate, might be related to the denser packing of these carbon nanostructures, as demonstrated by SEM images (Fig. 4) and particle size measurements. After exfoliation, particle association decreased because of the opening of the pore structure and, after reduction, the particle size increased again, thus corroborating the carbon lattice rearrangement.

The mechanism proposed for the oxidation and cutting of CNFs is based on the one proposed by Li et al. [29]. Firstly, K^+ ions and solvated SO_4^{2-} ions (or NO_3^-/ClO_4^- in the case of CNFs oxidized using the chromate procedure) open up the defective sites at the edges and can even enter into the CNFs interspace through oxidation, which may in turn weaken the van der Waals forces between graphene layers in CNFs. Thus, the reactive MnO_4^- or FeO_4^{2-} with H_2SO_4 (or CrO_4^{2-} with HNO_3/$HClO_4$) would enter into the CNFs interspace and attack the carbon skeleton of the nanomaterial. Although this mechanism is still not clear (by different intricacies such as van der Waals interactions by changing conductivity, solvation energy, viscosity etc.), it is demonstrated here that the conditions used in the acid oxidation process based on the use of chromate in the presence of HNO_3 and $HClO_4$ are not sufficiently strong to attack the internal carbon structure of the nanomaterial (carbon skeleton). Note that the changes produced in the porous structure of the CNFs treated with chromate, as well as the changes in both crystallinity and morphology, were totally different from those observed with the other two oxidants. This behavior shows that the chromate oxidation procedure was too mild and did not affect the carbonaceous network, thus leading to much less marked changes in the starting material.

3.2. Dispersibility study

Dispersibility analysis of the resulting oxidized nanomaterials on epoxy resin (compared to other solvent such as polar water and non-polar decane) were performed in order to analyze how the oxidative treatment influence on the ability of the resulting material to form stable dispersions.

With the aim of categorize the material stability into the solvent, Dai et al. [40] used three ranges of Turbiscan Stability Index (TSI) values for the study of the stability on a matrix: TSI < 5, categorize a well dispersed material, TSI from 5 to 20 categorize a well dispersed material with deposits at the bottom of the flask and, TSI above 20 is applicable to sedimentary materials.

Fig. 5 shows the Turbiscan data obtained during 48 h after the nanomaterials were dispersed into the epoxy resin. All dispersions were found to be highly stable, with TSI values below 5–6. As observed, the best dispersion stability was obtained using the CNFs oxidized by the ferrate procedure. Thus, a two-steps sedimentation took place using the CNFs oxidized using permanganate; a first sedimentation step in which biggest particles are sedimented at the bottom of the flask, during the first 3 h. Then the dispersion continues stable for 12 h more and finally, in the second sedimentation step, after 16 h of dispersion, the smaller

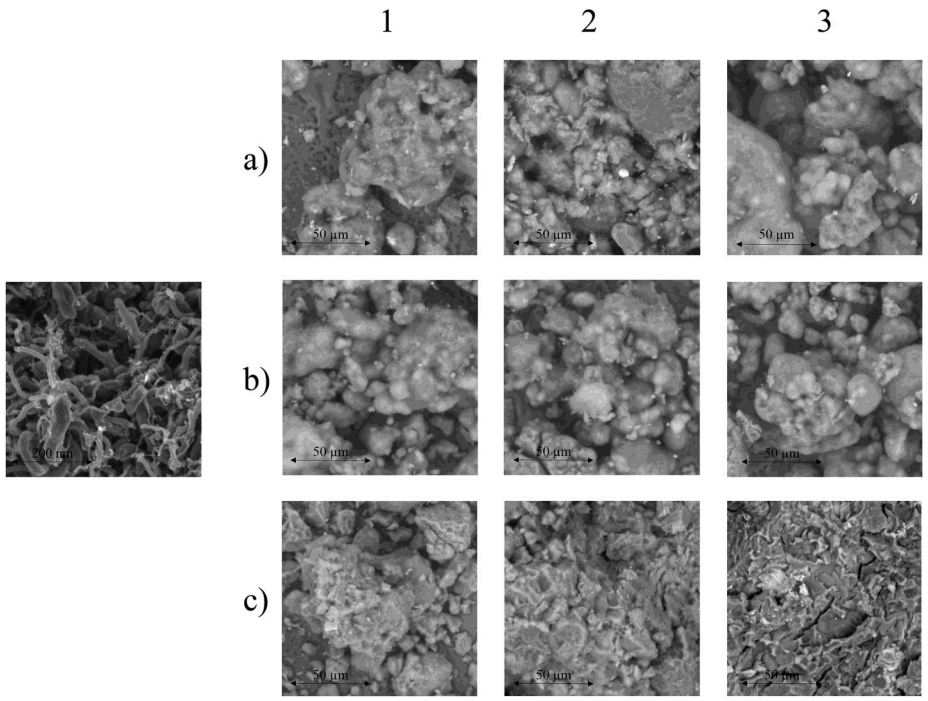

Fig. 4. SEM images of raw CNFs and samples: 1a) O-CNFs ferrate, 1b) O-CNFs chromate and 1c) O-CNFs permanganate; 2a) Ex-CNFs ferrate, 2b) Ex-CNFs chromate and 2c) Ex-CNFs permanganate; 3a) r-CNFs ferrate, 3b) r-CNFs chromate and 3c) r-CNFs permanganate.

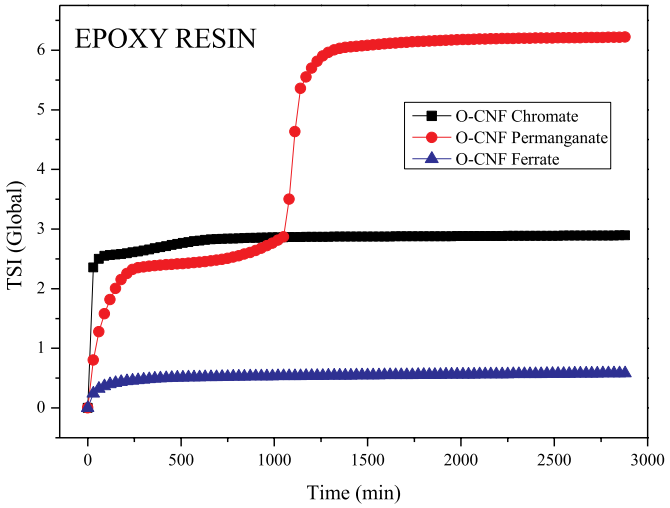

Fig. 5. Carbon samples TSI values dispersed on commercial epoxy resin.

particles start to precipitate, providing less stability to the dispersion and increasing the TSI value. On the other hand, samples oxidized by both chromate and ferrate showed a one-step sedimentation profile being more stable those dispersions with CNFs oxidized by ferrate with a TSI value around 0.5.

With the intent to focus on the dispersibility of those materials, two more solvents were studied: n-decane, a well-known non-polar solvent and water, the most common used polar solvent. Fig. 6, shows the Turbiscan data for those two solvents.

As expected, it was found that none of the oxidized CNFs could be well dispersed in n-decane due to its non-polar character, showing all dispersion high TSI values. Nevertheless, all the samples were well dispersed in water with TSI values below 5 points, value that represent a non-sedimentary system. In this case, the best stability results were obtained by the following order attending to the oxidizing agent: Permanganate > Ferrate > Chromate. As expected, those CNFs with more oxygen groups attached to the structure provided a better water dispersion stability due to the hydrogen-bonding interactions [40].

Taking into account the results, it seems clear that the chromate oxidation treatment of CNFs which introduce the lowest amount of oxygenated groups and prevent the destruction of the carbon skeleton, does not favor does not favor the formation of stable dispersions in any of the studied solvents (regardless of their polarity) if compared to ferrate and permanganate treated CNFs. The best dispersibility of these last samples, could be related to the nature of the functional groups present in the samples, in particular with the presence of epoxy groups, which were almost not appreciated in the chromate treated sample.

By its part, the anomalous behavior observed in the dispersion formed between the epoxy resin and the sample treated with permanganate, can be attributed to the significant increase in particle size that this sample experiences after the oxidation process, causing the larger particles to sediment in a period of time relatively short.

4. Conclusions

An exhaustive study was carried out that included the oxidation of carbon fiber nanostructures by different procedures with three different oxidation agents (potassium ferrate, chromate and permanganate), subsequent exfoliation and final reduction. The results clearly demonstrate that the different oxidizing strategies vary in their ability to oxidize CNFs effectively and, the nature of the oxygen functionalities attached to the carbon structure are different. It was demonstrated that significant differences exist between oxygen functional groups produced after oxidation using permanganate and ferrate procedures and those using the chromate procedure. The permanganate oxidation procedure led to a considerable increase in the amount of oxygen functional groups and this had a marked effect on the carbon skeleton of the raw CNFs and the textural properties of the material. Nevertheless, although these oxygen functional groups effectively promote polar interactions and hydrogen-bonding's which in turn favored stable epoxy dispersions, the high particle size of the oxidized sample caused the larger particles to sediment in a period of time relatively short.

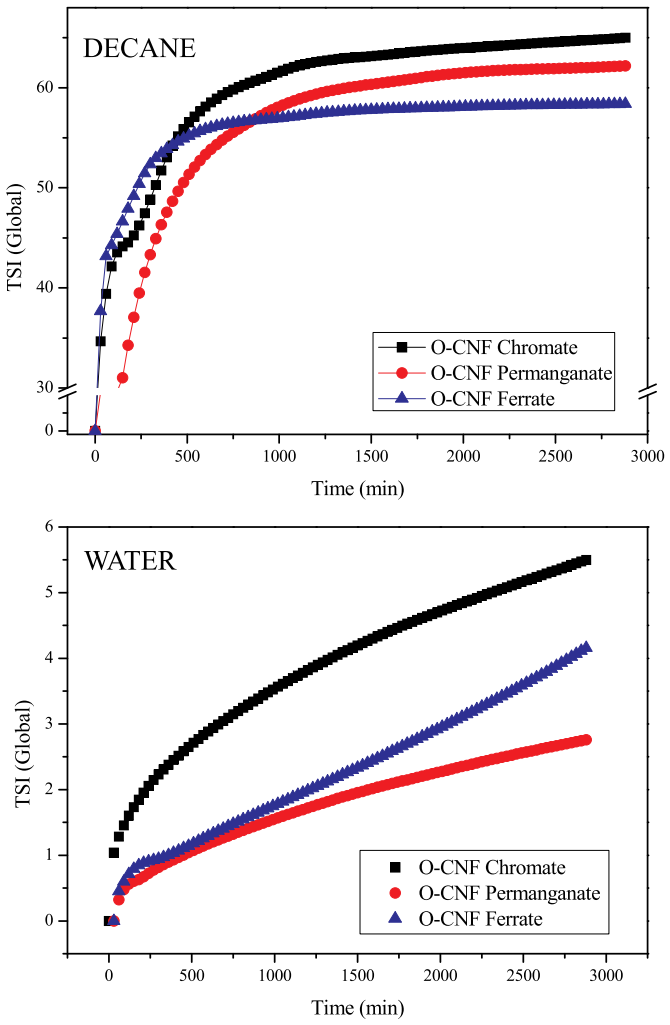

Fig. 6. Oxidized carbon samples TSI values dispersed on decane and water solvent.

Oxidation by the ferrate procedure proved to be quite similar to permanganate as far as the nature of the oxygen groups and the destruction of the carbon skeleton are concerned. Nevertheless, a lower oxidation degree was achieved with this method, modifying the textural properties but in lesser extent. The best results in terms of dispersion stability on polar solvents (water, epoxy resin), were obtained with this nanomaterial.

Finally, oxidation by chromate introduced the lowest amount of oxygenated groups into the CNFs although, it prevented the destruction of the carbon skeleton and thus had very little effect on the textural characteristics of the material.

In conclusion, different solution-based oxidative process was applied to CNFs. It was found that only those oxidation procedures in which H_2SO_4 was used (potassium permanganate and ferrate processes) were suitable to achieve the intercalation of suitable molecules (SO_4^{2-} ions) that weaken the van der Waals forces and make it possible for attack on the carbon skeleton by the strong oxidants MnO_4^- or FeO_4^{2-}.

Acknowledgment

The authors acknowledge financial support from the Spanish company Graphenano Nanotechnologies UCTR16017.

References

[1] A. Thakur, A. Manna, S. Samir, Direct growth of coiled carbon nanofibers without nanocatalyst, Diam. Relat. Mater. 74 (2017) 100–107, https://doi.org/10.1016/j.diamond.2017.02.011.
[2] A. Ramos, I. Cameán, A.B. García, Graphitization thermal treatment of carbon nanofibers, Carbon 59 (2013) 2–32, https://doi.org/10.1016/j.carbon.2013.03.031.
[3] C. Bao, Y. Guo, L. Song, Y. Kan, X. Qian, Y. Hu, In situ preparation of functionalized graphene oxide/epoxy nanocomposites with effective reinforcements, J. Mater. Chem. 21 (2011) 13290–13298, https://doi.org/10.1039/C1JM11434D.
[4] Y.J. Wan, L.C. Tang, L.X. Gong, D. Yan, Y.B. Li, L.B. Wu, J.X. Jiang, G.Q. Lai, Grafting of epoxy chains onto graphene oxide for epoxy composites with improved mechanical and thermal properties, Carbon 69 (2014) 467–480, https://doi.org/10.1016/j.carbon.2013.12.050.
[5] N. Domun, H. Hadavinia, T. Zhang, T. Sainsbury, G. Liaghat, S. Vahid, Improving the fracture toughness and the strength of epoxy using nanomaterials–a review of the current status, Nanoscale 7 (2015) 10294–10329, https://doi.org/10.1039/C5NR01354B.
[6] R. Joshua, O. Mamat, Z. Baig, Dispersion of Carbon Black in Epoxy Resin and the Electrical Property of the Nanocomposite, 2016.
[7] S.J. Park, Y.H. Chang, Y.C. Kim, K.Y. Rhee, Anodization of carbon fibers on interfacial mechanical properties of epoxy matrix composites, J. Nanosci. Nanotechnol. 10 (2010) 117–121, https://doi.org/10.1166/jnn.2010.1490.
[8] X. Qian, X. Wang, Q. OuYang, Y. Chen, Q. Yan, Surface structural evolvement in electrochemical oxidation and sizing and its effect on carbon fiber/epoxy composites properties, J. Reinf. Plast. Compos. 31 (2012) 999–1008, https://doi.org/10.1177/0731684412449895.
[9] J. Gulyás, E. Földes, A. Lázár, B. Pukánszky, Electrochemical oxidation of carbon fibres: surface chemistry and adhesion, Compos. Appl. Sci. Manuf. 32 (2001) 353–360, https://doi.org/10.1016/S1359-835X(00)00123-8.
[10] R. Whitby, V. Gun'ko, T. Fukuda, T. Maekawa, Relating bulk resistivity to nanoscale mechanical responses of carbon nanotubes randomly orientated in monoliths under compression, Carbon 48 (2010) 3635–3637, https://doi.org/10.1016/j.carbon.2010.05.021.
[11] H. Varela-Rizo, I. Rodriguez-Pastor, C. Merino, M. Terrones, I. Martin-Gullon, Graphene oxide nanoplatelets of different crystallinity synthesized from helical-ribbon carbon nanofibers and multiwall carbon nanotubes, J. Mater. Res. 26 (2011) 2632–2641, https://doi.org/10.1557/jmr.2011.272.
[12] J. Guerrero-Contreras, F. Caballero-Briones, Graphene oxide powders with different oxidation degree, prepared by synthesis variations of the Hummers method, Mater. Chem. Phys. 153 (2015) 209–220, https://doi.org/10.1016/j.matchemphys.2015.01.005.
[13] D.C. Marcano, D.V. Kosynkin, J.M. Berlin, A. Sinitskii, Z. Sun, A. Slesarev, L. B. Alemany, W. Lu, J.M. Tour, Improved synthesis of graphene oxide, ACS Nano 4 (2010) 4806–4814, https://doi.org/10.1021/nn1006368.
[14] M.d.P. Lavin-Lopez, A. Romero, J. Garrido, L. Sanchez-Silva, J.L. Valverde, Influence of different improved Hummers method modifications on the characteristics of graphite oxide in order to make a more easily scalable method, Ind. Eng. Chem. Res. 55 (2016) 12836–12847, https://doi.org/10.1021/acs.iecr.6b03533.
[15] M. Wojtoniszak, E. Mijowska, Controlled oxidation of graphite to graphene oxide with novel oxidants in a bulk scale, J. Nanoparticle Res. 14 (2012) 1248, https://doi.org/10.1007/s11051-012-1248-z.
[16] V. Jiménez, A. Nieto-Márquez, J.A. Díaz, R. Romero, P. Sánchez, J.L. Valverde, A. Romero, Pilot plant scale study of the influence of the operating conditions in the production of carbon nanofibers, Ind. Eng. Chem. Res. 48 (2009) 8407–8417, https://doi.org/10.1021/ie9005386.
[17] L. Peng, Z. Xu, Z. Liu, Y. Wei, H. Sun, Z. Li, X. Zhao, C. Gao, An iron-based green approach to 1-h production of single-layer graphene oxide, Nat. Commun. 6 (2015) 5716, https://doi.org/10.1038/ncomms6716.
[18] L. Stobinski, B. Lesiak, A. Malolepszy, M. Mazurkiewicz, B. Mierzwa, J. Zemek, P. Jiricek, I. Bieloshapka, Graphene oxide and reduced graphene oxide studied by the XRD, TEM and electron spectroscopy methods, J. Electron. Spectrosc. Relat. Phenom. 195 (2014) 145–154, https://doi.org/10.1016/j.elspec.2014.07.003.
[19] B. Warren, X-ray diffraction in random layer lattices, Phys. Rev. 59 (1941) 693, https://doi.org/10.1103/PhysRev.59.693.
[20] B. Fiedler, F.H. Gojny, M.H. Wichmann, M.C. Nolte, K. Schulte, Fundamental aspects of nano-reinforced composites, Compos. Sci. Technol. 66 (2006) 3115–3125, https://doi.org/10.1016/j.compscitech.2005.01.014.
[21] A. Romero, M. Lavin-Lopez, L. Sanchez-Silva, J. Valverde, A. Paton-Carrero, Comparative study of different scalable routes to synthesize graphene oxide and reduced graphene oxide, Mater. Chem. Phys. 203 (2018) 284–292, https://doi.org/10.1016/j.matchemphys.2017.10.013.
[22] D.R. Dreyer, S. Park, C.W. Bielawski, R.S. Ruoff, The chemistry of graphene oxide, Chem. Soc. Rev. 39 (2010) 228–240, https://doi.org/10.1039/B917103G.
[23] R.V. Hull, L. Li, Y. Xing, C.C. Chusuei, Pt nanoparticle binding on functionalized multiwalled carbon nanotubes, Chem. Mater. 18 (2006) 1780–1788, https://doi.org/10.1021/cm0518978.
[24] M. Li, X. Wu, J. Zeng, Z. Hou, S. Liao, Heteroatom doped carbon nanofibers synthesized by chemical vapor deposition as platinum electrocatalyst supports for polymer electrolyte membrane fuel cells, Electrochim. Acta 182 (2015) 351–360, https://doi.org/10.1016/j.electacta.2015.09.122.
[25] K.L. Klein, A.V. Melechko, T.E. McKnight, S.T. Retterer, P.D. Rack, J.D. Fowlkes, D. C. Joy, M.L. Simpson, Surface characterization and functionalization of carbon nanofibers, J. Appl. Phys. 103 (2008) 3, https://doi.org/10.1063/1.2840049.

[26] I.U. Din, M.S. Shaharun, D. Subbarao, A. Naeem, Surface modification of carbon nanofibers by HNO3 treatment, Ceram. Int. 42 (2016) 966–970, https://doi.org/10.1016/j.ceramint.2015.08.054.
[27] C.M. Yoon, D. Long, S.M. Jang, W. Qiao, L. Ling, J. Miyawaki, C.K. Rhee, I. Mochida, S.H. Yoon, Electrochemical surface oxidation of carbon nanofibers, Carbon 49 (2011) 96–105, https://doi.org/10.1016/j.carbon.2010.08.047.
[28] A. Rasheed, J.Y. Howe, M.D. Dadmun, P.F. Britt, The efficiency of the oxidation of carbon nanofibers with various oxidizing agents, Carbon 45 (2007) 1072–1080, https://doi.org/10.1016/j.carbon.2006.12.010.
[29] Y.-S. Li, J.-L. Liao, S.-Y. Wang, W.-H. Chiang, Intercalation-assisted longitudinal unzipping of carbon nanotubes for green and scalable synthesis of graphene nanoribbons, Sci. Rep. UK 6 (2016) 22755, https://doi.org/10.1038/srep22755.
[30] V. Datsyuk, M. Kalyva, K. Papagelis, J. Parthenios, D. Tasis, A. Siokou, I. Kallitsis, C. Galiotis, Chemical oxidation of multiwalled carbon nanotubes, Carbon 46 (2008) 833–840, https://doi.org/10.1016/j.carbon.2008.02.012.
[31] D. Torres, J. Pinilla, R. Moliner, I. Suelves, On the oxidation degree of few-layer graphene oxide sheets obtained from chemically oxidized multiwall carbon nanotubes, Carbon 81 (2015) 405–417, https://doi.org/10.1016/j.carbon.2014.09.073.
[32] A. Cuesta, P. Dhamelincourt, J. Laureyns, A. Martinez-Alonso, J.D. Tascón, Raman microprobe studies on carbon materials, Carbon 32 (1994) 1523–1532, https://doi.org/10.1016/0008-6223(94)90148-1.
[33] A. Dongil, B. Bachiller-Baeza, A. Guerrero-Ruiz, I. Rodríguez-Ramos, A. Martínez-Alonso, J. Tascón, Surface chemical modifications induced on high surface area graphite and carbon nanofibers using different oxidation and functionalization treatments, J. Colloid Interface Sci. 355 (2011) 179–189, https://doi.org/10.1016/j.jcis.2010.11.066.
[34] I.O. Maciel, N. Anderson, M.A. Pimenta, A. Hartschuh, H. Qian, M. Terrones, H. Terrones, J. Campos-Delgado, A.M. Rao, L. Novotny, Electron and phonon renormalization near charged defects in carbon nanotubes, Nat. Mater. 7 (2008) 878, https://doi.org/10.1038/nmat2296.
[35] M. Endo, K. Nishimura, Y. Kim, K. Hakamada, T. Matushita, M. Dresselhaus, G. Dresselhaus, Raman spectroscopic characterization of submicron vapor-grown carbon fibers and carbon nanofibers obtained by pyrolyzing hydrocarbons, J. Mater. Res. 14 (1999) 4474–4477, https://doi.org/10.1557/JMR.1999.0607.
[36] A.C. Ferrari, D.M. Basko, Raman spectroscopy as a versatile tool for studying the properties of graphene, Nat. Nanotechnol. 8 (2013) 235, https://doi.org/10.1038/nnano.2013.46.
[37] X. Wu, S. Mahalingam, A. Amir, H. Porwal, M.J. Reece, V. Naglieri, P. Colombo, M. Edirisinghe, Novel preparation, microstructure, and properties of polyacrylonitrile-based carbon nanofiber–graphene nanoplatelet materials, ACS Omega 1 (2016) 202–211, https://doi.org/10.1021/acsomega.6b00063.
[38] P. Hou, C. Liu, Y. Tong, S. Xu, M. Liu, H. Cheng, Purification of single-walled carbon nanotubes synthesized by the hydrogen arc-discharge method, J. Mater. Res. 16 (2001) 2526–2529, https://doi.org/10.1557/JMR.2001.0346.
[39] Y. Bai, Z.-H. Huang, F. Kang, Surface oxidation of activated electrospun carbon nanofibers and their adsorption performance for benzene, butanone and ethanol, Colloids Surf., A 443 (2014) 66–71.
[40] J. Dai, G. Wang, L. Ma, C. Wu, Study on the surface energies and dispersibility of graphene oxide and its derivatives, J. Mater. Sci. 50 (2015) 3895–3907, https://doi.org/10.1007/s10853-015-8934-z.